Waste and Biomass Valorization (2020) 11:5027–5039
https://doi.org/10.1007/s12649-019-00781-z

ORIGINAL PAPER

Effects of Activator Properties and Curing Conditions on Alkali-Activation of Low-Alumina Mine Tailings

Mahroo Falah[1] · Robert Obenaus-Emler[2] · Paivo Kinnunen[1] · Mirja Illikainen[1]

Received: 11 April 2019 / Accepted: 6 August 2019 / Published online: 13 August 2019

Abstract

The mining industry generates a notable amount of mine tailings (MTs). Disposal of MTs creates environmental impacts such as air pollution and the release of heavy metals into surface and underground water. The European Union (EU)-funded project "Integrated mineral technologies for more sustainable raw material supply" (ITERAMS) includes an effort to produce eco-friendly backfill materials to enhance operation and mine safety and covers for surface deposits of tailings based on geopolymerization technology. This paper investigates the effects of activator concentration, curing temperature and time on alkali-activated materials based on low-alumina MTs from the Cu/Ni mine in Northern Finland. Alkaline activators containing sodium silicate solution (Na_2SiO_3) at different concentrations were used and two different curing temperatures, 40 °C and 60 °C, for periods of 7, 14, and 28 days were considered. Scanning electron microscopy/energy-dispersive X-ray spectroscopy (SEM/EDS) and X-ray diffraction (XRD) were performed to investigate the structure, morphology and phase compositions of the alkali-activated products. The effect of curing temperature and alkaline solutions on mechanical strength and water absorption were investigated. The results indicate that the alkalinity and curing temperature affect the mechanical and microstructural properties of the compositions of alkali-activated MTs. The 30 wt% Na_2SiO_3 addition enables the alkali activated MT to improve the compressive strength with a highest value of 6.44 and 15.70 MPa after 28 days of curing at 40 °C and 60 °C, respectively. The results of this study deliver useful information for recycling and utilization of MTs as sustainable material through the alkali activation.

Graphic Abstract

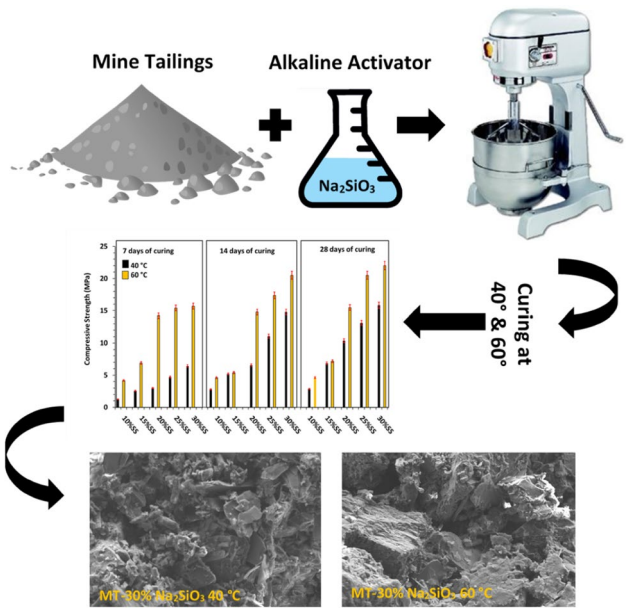

Extended author information available on the last page of the article

Keywords Mine tailings · Alkali activation · Curing condition · Mechanical strength · Microstructure

Statement of Novelty

This work reports the development of a new category of alkali activated materials with special low alumina mine tailings for control of environmental pollution. The final products have been produced based on alkali activation process with an available mine tailing. The novel aspect of this work is modification of the low-alumina mine tailings by the insertion of sodium silicate, giving the alkali activated products enhanced strength properties when compared with raw materials before activation process. The excellent efficiency of these new materials makes them potentially useful candidates for the control of airborne environmental pollutants.

Introduction

The mining industry creates a huge amount of mine tailings (MTs) each year [1, 2]. MTs are crushed rock deposits left over after the metal-bearing minerals have been extracted from the ore [3]. MTs are made into a slurry or paste and then transported to on-site impoundments behind rock dams or stacked in tailings storage areas. The huge amount of MTs produced by mining operations and caused environmental and safety problems, including serious water pollution. The pollution raised up from contamination of surface water, groundwater, and soils by the leaching of heavy metals, and sulphur compounds [4].

Developing cost-effective and environmentally acceptable strategies for the disposal of such waste has thus become critical for the productivity of mining operations. There are different approaches to reduce the potential environmental hazards related to MTs: (i) isolation of MTs, which includes isolation of MTs from the nearby environment by capping the tailing impoundment surface (ii) chemical stabilization of MTs by chemical or cementitious material additions in order to immobilize the heavy metals through physical–chemical reactions, and (iii) a combination of these two methods. For the simultaneous use of isolation and stabilization techniques, the tailing surface can be treated with additives such as water glass (Na_2SiO_3), organic polymers, and Ordinary Portland Cement (OPC). The effect of additives cause an improvement at the surface erosion resistance and reduce water penetration, which led to isolates the underlying tailings from the surrounding environment [5–7]. Although OPC recommends benefits in the stabilization of MTs, there are still some problems such as high energy consumption and CO_2 emissions which are related to the OPC addition.

Geopolymerization or alkali-activation of tailings has been suggested in place of a promising method for immobilizing the tailings as a raw material for construction. Through alkali-activation, different raw materials can be transformed into valuable cementitious-like materials with low environmental impact. Geopolymers not only deliver comparable performance to OPC in many applications, but also have additional advantages, such as excellent devotion to aggregates, rapid development of mechanical strength, high acid resistance, immobilization of toxic and hazardous materials, and a considerable reduction in greenhouse gas emissions [3, 8, 9].

Generally, geopolymers are formed from the reaction of aluminosilicate minerals and silicate or alkaline hydroxide solution [3, 10]. Until now, the research on geopolymers has been concentrated on the utilization of kaolinite, fly ash, and blast furnace slag as the aluminosilicate source material. Different parameters, such as activator type and concentration [11, 12], curing process, and the composition of aluminosilicate sources, [13] considerably influence the geopolymerization processes and the final specifications of geopolymers. Sodium silicate solutions are identified to have a notable impact on the dissolution performance and precipitation characteristics of geopolymers, by enhancing alkali-metal attack on aluminosilicate particles and consequently accelerating geopolymer formation [14, 15]. It is also known that using a silicate activating solution instead of a hydroxide have possibility of controlling the geopolymerization process, strength development in geopolymeric binders, and the microstructure of the activated products [16–18]. Beyond the ideal alkaline solution and concentration, the geopolymer curing condition have a significant effect on microstructural and mechanical strength development in cementitious systems alkali activated process [6]. Curing at higher temperatures leads to produce a fast geopolymerization process to achieve an acceptable strength within very short periods.

Recently, one-part alkali activation process received a great attention. One-part alkali activation involves a dry mix, contains different precursors and solid alkali sources, and then water addition, which is similar to preparation of the commercial cementitious materials [19–23]. Regardless of all proposed environmental and economic benefits of alkali-activated binders, there are some difficulties for these binders such as large drying shrinkage and efflorescence. In order to minimize the problems, different methods have been proposed. The methods include using thermal curing, different additives, and fibers [24–33].

Currently, an increasing interest in recycling of mine tailings as raw materials for producing geopolymers have

been developed. However research on geopolymerization or alkali-activation of MTs is still in its initial stages. Until now, Zhang et al., Ahmari et al., and Li et al. [1, 3, 4, 7, 34–37] have studied the effect of different factors (i.e., activators and curing temperature) on alkali-activated binders based on copper MTs and confirmed the MT wastes can be used as an alternative raw material for the preparation of geopolymer. Torgal et al. [38] first emphasised the possible use of a combination of calcined tungsten mining waste (TMW) mud and calcium hydroxide for the improvement of a high early strength geopolymeric binder, and Kiventerä et al. [39] have investigated the effect of using sulphide mine tailings as suitable raw materials for alkali activation purposes. They concluded the sulfidic mine tailings could be activated with the addition of low amount (5 wt%) of blast furnace slag as a co-binder. They also studied the immobilization of heavy metals in alkali-activated materials [40, 41]. However, none of the previous studies have investigated the reusing of low alumina mine tailings for alkali activation process and geopolymerization. Furthermore, using of MT as precursor for the alkali activation process to make a backfill materials and cover layer surface has not been considered.

The main purpose of this study is to investigate the effects of using different alkali activator concentration, curing temperature and time on the morphology, elemental composition and mechanical properties of the selected low alumina-MTs. This paper studies the feasibility of alkali-activated mine tailings (AAMTs) with different percentages of Na_2SiO_3 solution. Different factors, such as curing temperature and curing time, are examined on the AAMTs with different Na_2SiO_3 concentrations. Compression tests are conducted to investigate the mechanical properties of AAMTs produced at different conditions. Scanning electron microscopy (SEM) imaging and X-ray diffraction (XRD) analyses are also performed to investigate the microstructure and material phases of AAMTs. Furthermore, a detailed microstructural characterization of the final products was conducted to help understand the origin of the properties of the resulting products. It should be noted that this research is an initial experiment which carried out at different curing temperatures to improve the reaction speed. Further experiments will be done at room temperature and expected to achieve the same results specifically similar strength but with slower reaction and in the longer curing time.

Materials and Mix Design

Materials

MTs were supplied by Cu/Ni mine in Northern Finland in the Lapland province. Sodium silicate solution (from VWR chemicals) with a modulus of 3.2 ($Ms = SiO_2/Na_2O$) and water content of 55% was selected as an alkali activator. The chemical composition of the MTs was determined by X-Ray fluorescence (Axios mAX; Malvern PANalytical) equipped with a rhodium tube with a maximum power rating of 4 kW. In relation to the chemical compositions, the MT was rich in Magnesium (MgO: 21.82 wt%) and the amounts of silica (SiO_2: 47.96 wt%), iron (Fe_2O_3: 12.06 wt%), and calcium (CaO: 11.28 wt%) were significant. Additionally, the tailings have a considerably low amount of alumina (Al_2O_3: 3.99 wt%).

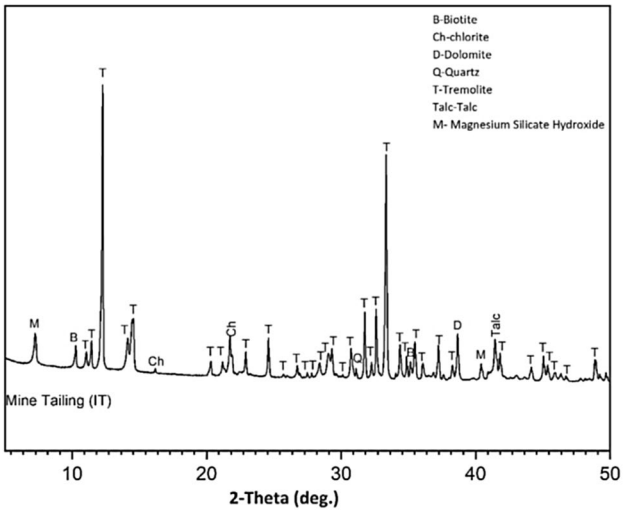

Fig. 1 XRD (Cu K_α radiation) patterns of Mine Tailing

Figure 1 shows the mineral compositions of oven-dried MT tested by X-ray diffraction (XRD) using Rigaku SmartLab 9 kW with Cu Kα (Kα1 = 1.78892 Å; Kα2 = 1.79278 Å; Kα1/Kα2 = 0.5) radiation operated at 45 kV and 40 mA, with a step of 0.02° and a scan rate of 3°/min from 5° and 90° (2θ). Phase identification was performed by using X'pert HighScore Plus (PANanalytical software for XRD characterization). The mine tailing contains certain amounts of crystalline phases, including tremolite ($Ca_2Mg_{4.95}Fe_{0.05}\ Si_8O_{22}(OH)_2$, JCPDS# 01–085-0876), chlorite ($Mg_{4.6}Fe_{0.55}Al_{1.7}Si_{3.15}O_{10}(OH)_8$, JCPDS# 01–083-1381), quartz (SiO_2, JCPDS# 00–033-1161), talc ($Mg_3Si_4O_{10}(OH)_2$, JCPDS# 00–019-0770), magnesium silicate hydrate ($H_2Mg_2O_9Si_3$, JCPDS# 01–078-2611), dolomite ($CaMg(CO_3)_2$, JCPDS# 00–036-0426) and calcite ($CaCO_3$, JCPDS# 00–005-0586).

Particle size analysis of the powdered material (MT) was performed with LS 13 320 laser diffraction particle size analyzer from Beckman Coulter using the Fraunhofer model [42]. In order to increase the reactivity of the mine tailings and thus increasing the ultimate strength of the alkali-activated materials, different approaches were successfully tested. The thermal treatment of the MT showed that the reactivity of the material can be increased by calcination at

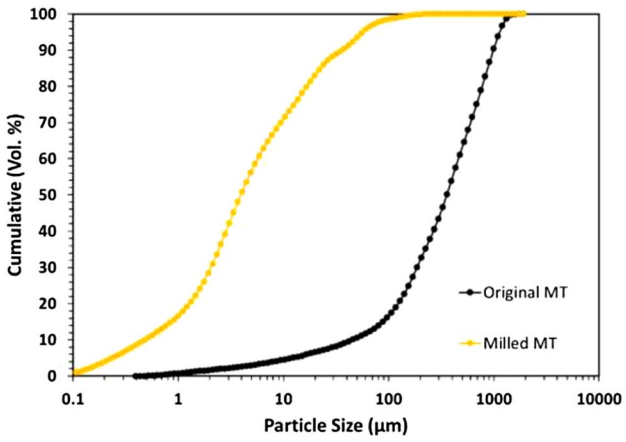

Fig. 2 Particle size distribution of MT

temperatures above 700 °C which is most likely linked to the dehydration of chlorite. Since calcination is an energy intense process and requires large investment, this procedure was not further investigated in this study.

For the further synthesis, the MT was sieved and milled to achieve a grain size of less than 5 µm. The milling of the material was produced by using a vibratory disc mill (RS 200) for 30–60 s to accomplish the preferred particle size. The MT had a d_{50} value and density of 422.12 µm and 3.05 g/cm^3, respectively. Although the milling process could be cost effective in the mine site but according to some mineralogical analysis of the MT, a higher specific surface area should increase the dissolution rate and consequently a faster hardening for the alkali activated final products. Figure 2 displays the particle size distribution curve of the MTs before and after grinding.

Specimen Synthesis and Curing

The alkali-activated mine tailings (AAMTs) were prepared by adding the activator solutions to the solid materials. The molarity of the alkaline activator solution was 6 and additional water was added to the mixture to achieve the desired slurry concentration. The MTs were mixed with 10, 15, 20, 25, and 30 wt% of the Na_2SiO_3 solution, and then water was added to the mixture to adjust the liquid-to-solid mass ratio to 0.23. The slurry was stirred for another 5 min, transferred to prismatic beam molds (20×20×80 mm), and vibrated for 60 s on a vibrating table. The fresh pastes were then sealed in plastic and subjected to cure for 24 h at 40 °C and 60 °C. The specimens were then de-molded, unsealed, and subjected curing at 40 °C and 60 °C for 7, 14, and 28 days. The recipes for the mixtures are provided in Table 1. The samples are designated as MT, MT-NA x[%, where x% refers to the weight% Na_2SiO_3 content of the AAMT.

Table 1 The Proportions of the mix compositions

Mixtures	MT (%)	Sodium silicate (%)	Water/binder
MT-NA-10%	90	10	0.29
MT-NA-15%	85	15	0.29
MT-NA-20%	80	20	0.29
MT-NA-25%	75	25	0.29
MT-NA-30%	70	30	0.29

Regarding the use of the five different percentages of the activator additives (10, 15, 20, 25, and 30 wt% of the total solid mass), a total of 30 prismatic beams were prepared and then tested to measure the compressive strength. Three or four specimens were tested for each mixture at different curing conditions to give average values.

The following properties were determined after curing: phase analysis, morphology and micro-structure, water absorption, and mechanical strength.

Characterization

Three-Point Bending Test (TPB)

In total, 30 prismatic beams with dimensions of 20×20×80 mm were used to measure the flexural behaviour of the beams made with MTs and alkali activated materials under a three-point bending (TPB) test in agreement with the ASTM C293 recommendation [43].

The flexural load was recorded by using a wick, Z100 Roell testing machine with a load cell of 100 kN capacity. For each mix composition which prepared at different curing conditions three prismatic beams were tested with a constant flexural load speed of 0.6 mm/min. The flexural load was submitted to the beams under a displacement control. The flexural strength of specimens calculated by using the Eq. (1) under the TPB test:

$$Q_f = \frac{3FL}{2bh^2} \quad (1)$$

where F is the total flexural load, L is span length, b and h are width (20 mm) and height (20 mm) of beams, respectively.

Compressive Test

The compressive strength of the specimens was measured conferring the ASTM C116-90 by using the portions of prismatic beams broken in flexural tests [44]. The compressive load was measured using a testing machine (Z100; Zwick-Roell) with a maximum load capacity of 100 kN. All the broken prismatic beams were measured under a compressive load with a constant displacement rate of 2 mm/min. The compressive strengths of the mixtures were obtained

by averaging the values obtained for the six prisms (3 × ½ prisms).

Microstructural Analysis

To examine the phase morphology and microstructure evolution, selected crushed and dried specimens were observed by field emission scanning electron microscopy (FE-SEM) (Ultra Plus; Zeiss) fitted with an electron dispersive x-ray spectroscopy (EDS). An accelerating voltage of 15 keV was used to analyze the structural and chemical texture of the samples. The samples were carbon-coated with a 7–9 nm carbon layer.

Water Absorption

The effect of water absorption on AAMTs was investigated in agreement with BS EN ISO 62:1999 [45]. Overall, 15 prismatic beams (20×20×80 mm) were prepared and cured for 28 days using the procedure mentioned at Sect. 2.2 The prismatic bar specimens were immersed in a water bath at 23 °C for 24 h. Then, the specimens were removed from the water and the surface water was removed by wiping with a clean dry cloth. The wiped specimens were then weighed again in one minute after removing from water. All specimens were heated by using an oven at 105 ± 2 °C for 24 h, the masses of the cooled specimens checked to reach a constant mass. The water absorption capability was defined by using the following Eq. (2):

$$W_{abs}(\%) = \frac{W_s - W_D}{W_D} \times 100 \quad (2)$$

where W_a is water absorption, W_f is the weight of specimen after immersion (g), and W_i is the mass of the dried specimens (oven-dry weight) (g).

Results and Discussion

XRF Analysis

The chemical compositions of the treated MTs before and after activation with Na_2SiO_3 are presented in Table 2. Concerning the chemical compositions, the alkali activation process happened, so then the composition of the AAMTs changed. The increase in Na and Si with increasing sodium silicate content is reasonable but the change in the Fe and Mg contents is related to the uncertainty of the analysis.

XRD Analysis

A selection of representative powder XRD patterns of the MT activated by different sodium silicate contents at the age of 28 days and curing of 40 °C are shown in Fig. 3. The patterns of the alkali-activated product of the five MT-Na specimens can be classified into two types: (a) patterns with the peaks that are remnant from parent MT and (b) patterns with the peaks that are formed during alkali activation. Apart from tremolite, chlorite, quartz, talc, calcite, and magnesium silicate hydrate which released from raw materials, calcium silicate hydrate ($Ca_2SiO_4.H_2O$ (C–S–H), JCPDS# 00-003-0649) and new peak of magnesium silicate hydrate in the AAMTs can be identified. The generation of C–S–H is due to the combination of soluble Ca^{2+} ions from MTs and SiO_4^{4-} ions from alkaline solution during the alkali activation process. The Ca provided from CaO contents in the precursor materials (MT) and sodium silicate are responsible for providing a soluble silica. Presence of small new peak of calcite is related to the rapid dissolving of Ca in the alkaline solution and precipitation of $Ca(OH)_2$, finally transforming into calcite [38, 39, 41]. In AAMTs (Fig. 3), the C–S–H peak is shown at near 28° 2θ, resembling the diffraction pattern of a poorly ordered calcium silicate hydrate (C–S–H). The reason of not having a sharp peak of C–S–H is probably due to the lack of enough silicon inside or because of the lower quantity detection limit of the XRD instrument. Calcite peaks do not show any differences in intensity at the mix compositions with different sodium silicate contents, this is suggesting an attendance the residue of untreated MTs.

The XRD patterns for the AAMT cured at 60 °C for 28 days keep the same crystalline peaks as the peaks released in the 40 °C cured samples. It should be noted that there is no difference realized even in the XRD pattern of the samples cured at room temperature which indicates that the major constituent of the alkali activation process happened at ambient temperature and the XRD patterns of the AAMTs

Table 2 Chemical Composition (% by Weight) of materials as determined by XRF

Mixture	Na_2O	MgO	Al_2O_3	SiO_2	P_2O_5	SO_3	K_2O	CaO	TiO_2	MnO	Fe_2O_3	CuO	NiO	ZnO	Cl
MT	0.58	21.82	3.99	47.96	0.02	0.15	0.23	11.28	0.37	0.17	12.06	0.13	0.05	0.01	0.05
MT-NA-10%	0.98	21.26	3.31	48.26	0.02	0.68	0.35	12.55	0.32	0.17	11.09	0.12	0.04	0.01	0.06
MT-NA-15%	1.30	21.04	3.47	48.57	0.02	0.71	0.26	11.82	0.31	0.16	11.05	0.11	0.04	0.01	0.06
MT-NA-20%	1.64	20.88	2.70	48.79	0.01	0.98	0.37	13.29	0.27	0.15	10.82	0.10	0.03	0.01	0.05
MT-NA-25%	1.94	20.65	2.75	48.82	0.01	1.06	0.34	12.95	0.30	0.16	10.77	0.10	0.03	0.01	0.05
MT-NA-30%	2.03	20.40	3.03	49.15	0.02	0.81	0.30	12.30	0.30	0.17	10.61	0.10	0.03	0.01	0.06

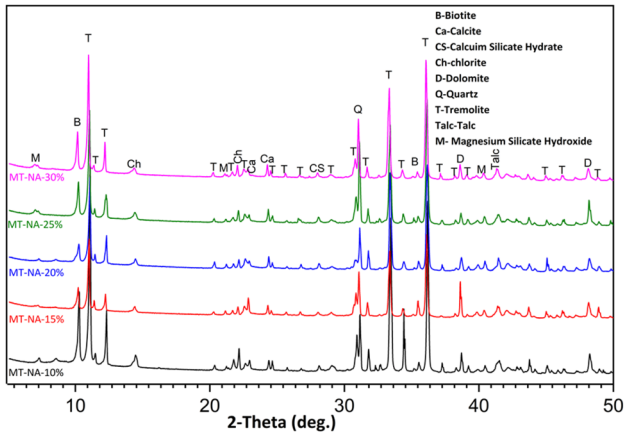

Fig. 3 XRD patterns of the 28-days cured AAMT containing (10–30 wt%) Na_2SiO_3 solution

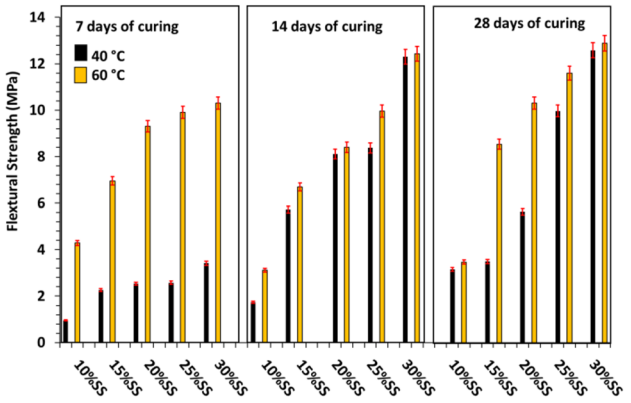

Fig. 4 Flexural strength of AAMT at 7 days, 14 days and 28 days

remained unchanged even after increasing the curing temperature (60 and 40 °C).

Flexural Strength of AAMT

The influences of different contents of Na_2SiO_3, curing time and temperature on the flexural strength are illustrated in Fig. 4. Increasing the addition of Na_2SiO_3 increased the flexural strength, and the maximum flexural strength was recorded in the mixture of MT-30% Na_2SiO_3 at 60 °C for 28 days (around 13 MPa). At the early curing time (7 days), the maximum flexural strength is attributed to the mix composition have been cured at 60 °C (around 10 MPa), and the minimum was related to the mixture incorporating 10% Na_2SiO_3 and have been cured at 40 °C.

According to the results presented in Fig. 4, regardless of sodium silicate content, specimens cured at 60 °C and 40 °C showed the maximum and minimum flexural strength,

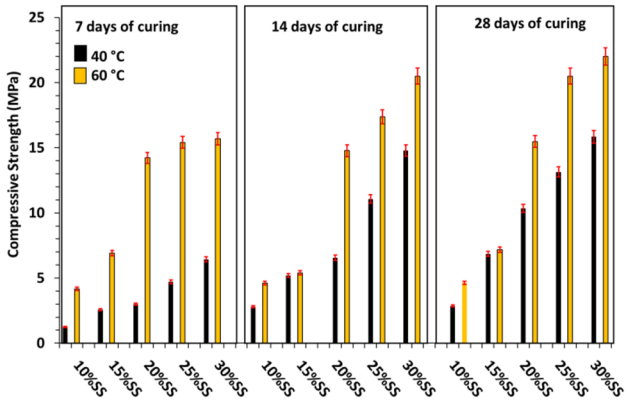

Fig. 5 Compressive strength of AAMT at 7 days, 14 days and 28 days

respectively. This outcome could be explained by the effect of curing conditions on polycondensation process.

Moreover, using higher amount of sodium silicate led to slightly higher flexural strength which could be described by the formation of more reaction products. Through increasing in the curing time from 7 to 28 days a strength improvement was distinguished in the mixtures, which was governed by the curing approach. Ghafoori et al. and Abdollahnejad et al. [20, 46] showed a comparative study to evaluate the effects of using different curing conditions in geopolymers and one-part alkali-activated waste binders.

Compressive Strength of AAMT

The compressive strength of AAMT specimens cured at 40 °C and 60 °C for 7, 14, and 28 curing days containing different Na_2SiO_3 addition of 10, 15, 20, 25, and 30 wt% are shown in Fig. 5. As indicated in Fig. 5, the highest 7-day compressive strength was detected at the 30 wt% addition of the alkali-activated additives, where the maximum compressive strengths are 6.44 and 15.70 MPa for the samples cured at 40 °C and 60 °C, respectively. According to the mining requirements, the ultimate strength of backfill materials can range from 0.2 to 5 MPa and the rapid strength development as more than 2 MPa for the first 7 days after installation are required. A desirable condition for the installed covering layer is mainly focused on the flexibility and permeability of the surface. The minimum 7 day compressive strengths were found at the 10 wt% Na_2SiO_3 addition with 1.24 and 4.17 MPa strength for curing at temperatures of 40 °C and 60 °C, respectively.

This result indicates that the compressive strength increases with increasing of the activator addition (Na_2SiO_3 here) and curing temperature. Similarly, the maximum 14 and 28 day compressive strengths were also noticed at the 30 wt% addition of Na_2SiO_3 for both 40 °C and 60 °C curing conditions. At 40 °C and 60 °C curing temperatures, the 14 day compressive strengths are 14.78

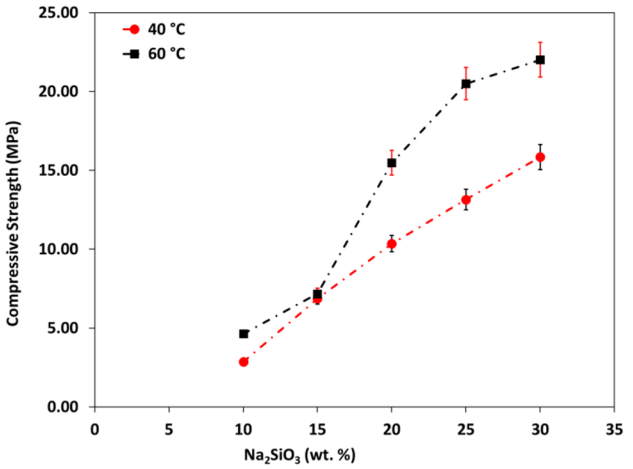

Fig. 6 Compressive strength with different Na_2SiO_3 concentrations for the specimens cured at 40 °C and 60 °C for 28 days

and 20.49 MPa, correspondingly (Fig. 5), and the 28 day compressive strengths are 15.84 and 22 MPa for a 30 wt% activator addition at 40 °C and 60 °C curing temperatures, respectively (Fig. 5).

The strength difference between curing at 60 °C and curing at 40 °C is higher for the shorter curing time (7 days) than for 14 and 28 days. This indicates a faster reaction rate at a higher temperature in a shorter curing time. The final strength of the product at 60 °C is obtained somewhere between 14 and 28 days, while it took a little longer for the sample cured at a lower temperature (40 °C) to reach the same strength level. This could be related to the hydration process for that special AAMT that needs longer time in lower temperatures to be completed.

Furthermore, the strength and compressibility of the MT treated with Na_2SiO_3 solution is related to the structure as confirmed with microstructure analysis (Figs. 6 and 8). In general, the highest strength of all mixes was attained with the addition of 30 wt% of Na_2SiO_3 solution at 60 °C curing condition.

It is obvious from the test results that increasing the activator solution content from 10 to 30 wt% not only increases the compressive strength of the specimen at a selected curing temperature but also increased strength with time (Fig. 5). It should be noted that the curing time and temperature have a significant impact on mechanical strength development.

It is worth mentioning this research was an initial experiment for investigating the feasibility of alkali activation of the selected low alumina MT. The selected curing temperatures used for the speed up the reaction and further analysis will be done in an ambient temperature based on the field requirements.

Figure 6 shows the variation of compressive strength achievements with curing temperatures at different additions of Na_2SiO_3 contents. The effect of Na_2SiO_3 contents on the compressive strength depends on the curing temperature. At a curing temperature of 40 °C, the compressive strength slightly increases with greater Na_2SiO_3 addition. At a curing temperature of 60 °C, there is an increase in the compressive strength when the Na_2SiO_3 addition increases from 10 to 30 wt%. Temperature speeds up the alkaline activation of a solid mixture as it happens with most of the chemical reactions. Equally when temperature increases, the rate of the reactions increases.

SEM/EDS Analysis of the AAMT

The effect of using various amount of Na_2SiO_3 on the morphology of specimens cured at 40 °C for 28 days is indicated in Fig. 7(b–d). Figure 7a shows that the MT particles have irregular shapes with the rough surface, and the fine particles are attached to the surface of coarse particles. It is obvious, the addition of Na_2SiO_3 greatly impacted the matrix morphologies and increased the degree of reaction, which made the matrix denser and resulted in an improvement in the compressive strength. The unreacted MT particles were highlighted in the AAMT contains 10% Na_2SiO_3 (Fig. 7b), indicating a lower degree of dissolution of MT and alkali-activated materials. The matrix of the AAMT with 30% Na_2SiO_3 was almost entirely transformed into fused rectangular prisms, which indicates a more complete transition in high-alkaline conditions. EDX analysis demonstrated that sodium silicate addition led to an increase in the Si/Al, Si/Ca and Mg/Al contents (see Table 3). Lower Ca/Si molar ratios result in the formation of higher strength stability and illustrated a higher degree of alkali activation process. This is perhaps a result of improvement in the final strength of the sample contains more Na_2SiO_3.

The microstructure of MT with a 30 wt% Na_2SiO_3 content (Fig. 7d) reveal a morphology consisting of a random array of sheet-like un-aggregated particles corresponding to the identified phases by XRD. The structure appeared to be more homogenous and denser, which is due to the dissolution of available silica, magnesia, and calcium in the mixture. Moreover, with increase in Na_2SiO_3 content, the flocculated nature of the structure and the areas of flatness in the structure become more obvious.

Alkaline solution plays two important roles during alkali activation process, dissolution of silica species and increasing pH, and charge-balancing by providing the presented metal cations [47]. The current experimental results show an increase in compressive strength with Na_2SiO_3 concentration. The increase in compressive strength with higher Na_2SiO_3 concentration is due to the presence of more silica components and thus incorporation of larger quantities of silica components in the activation process. However, the current experiment indicates that the compressive strength

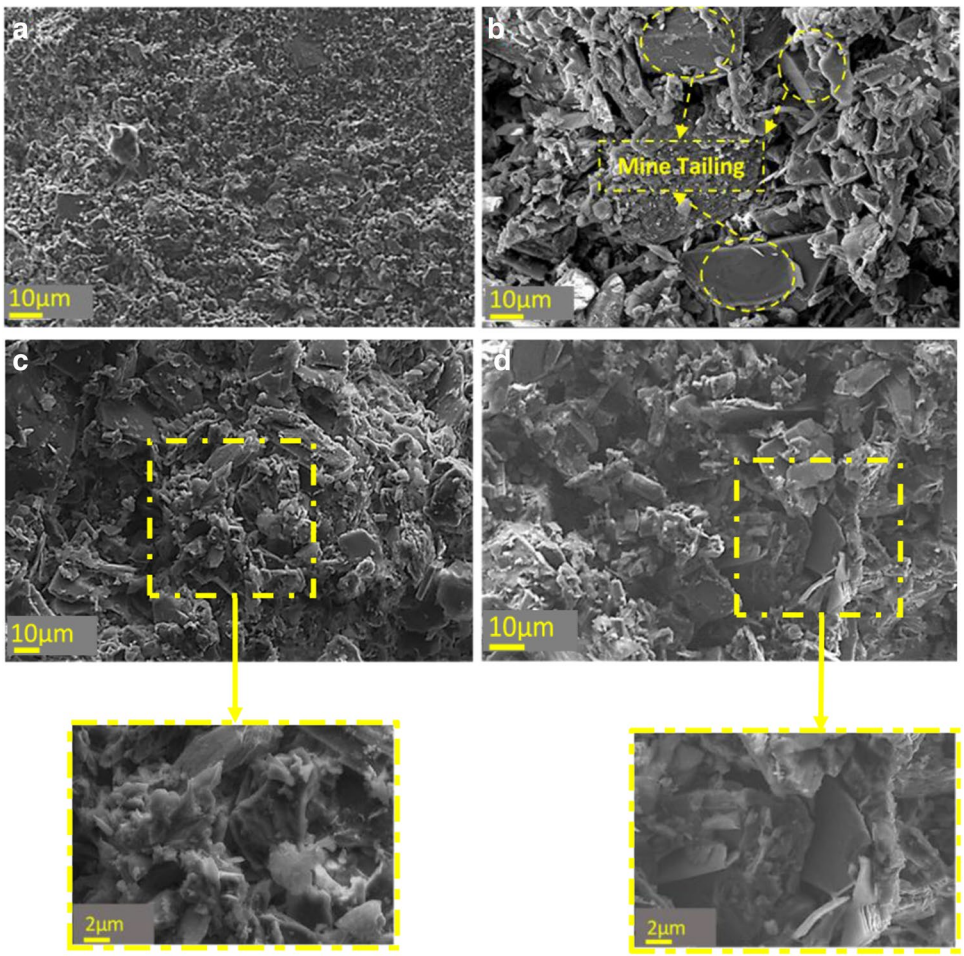

Fig. 7 Representative SEM micrographs of **a** MT, **b** MT-NA-10%, **c** MT-NA-20% (highlighted area with higher magnification) and **d** MT-NA-30% (highlighted area with higher magnification) cured at 40 °C for 28 days

Table 3 The EDX atomic ratio analysis

Mixture	SiO_2/Al_2O_3	Al_2O_3/Na_2O	CaO/SiO_2	SiO_2/CaO	Na_2O/CaO	MgO/Al_2O_3
MT	10.19	2.80	4.22	0.01	23.91	0.24
MT-NA-10%	17.65	1.52	0.25	4.14	0.15	7.61
MT-NA-15%	21.67	0.45	0.24	4.03	0.41	7.73
MT-NA-20%	21.70	0.48	0.21	5.07	0.50	8.29
MT-NA-25%	29.04	0.49	0.20	5.01	0.51	11.26
MT-NA-30%	38.18	0.49	0.19	5.39	0.53	13.68

increases with alkalinity, which is possibly due to the dissolution of crystalline silica, calcium, and magnesium to form C–S–H or M–S–H, this result is in agreement with XRD analysis.

However, the Ca/Si ratios are in the range of 0.1–0.34 which are obviously lower than the value of 0.67 usually reported for C–S–H [48]. Lower Ca/Si atomic ratios result in the formation of a denser matrix and higher strength stability. A low Ca/Si ratio led to a higher degree of alkali activation process. It could be due to the incorporation of magnesium in calcium silicate hydrate because the presence of notable amount of magnesium in the mixture. The presence of other compounds, such as Mg, during the alkali activation process can induce modification in the hydrated product, for instance the incorporation of Mg^{2+} into the structure. Pytel [49] and Fernandez et al. [50]. identified the possible incorporation of magnesium into the CSH structure and observed a new phase attributed to the formation of a magnesium silicate hydrate (MSH). MSH gel formation is only considered into the CSH gel of low CaO/SiO_2.The existence of different silicate structure prevents the formation of M–C–S–H phase but leads to the presence of separate M–S–H and C–S–H phases in the mixture containing magnesium and calcium [48, 51].

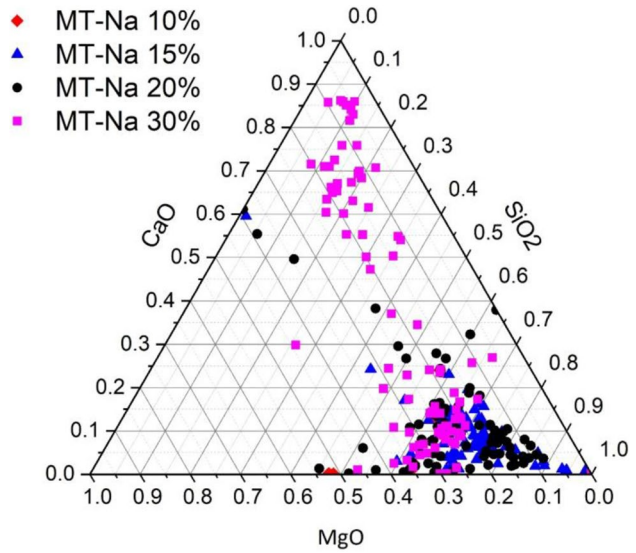

Fig. 8 Ternary diagram for the MgO–SiO_2–CaO–H_2O system showing the AAMTs in the presence of silicates containing magnesium and/or calcium

The improving effect of high alkalinity on the compressive strength can be described by the presence of sufficient calcium and formation of C–S–H as a result of higher alkalinity concentration, which has been reported by different researchers [52–57]. The formed C–S–H gels block the voids in the matrix and make a stronger microstructure [56, 57].

A schematic illustration of the phase relations in the system of MgO–SiO_2–CaO–H_2O, including specimens contain 10, 15, 20 and 30 wt% Na_2SiO_3 is given in the ternary diagram of Fig. 8. The composition of the hydrated phase has been projected on to the anhydrous base of the system. Each point has been plotted from EDX analysis of Table 3. The M–S–H (MgO–SiO_2 binary system) and C–S–H are included and confirmed the composition of the AAMTs. The samples are nearer to the chemical composition of C–S–H than M–S–H and this can be deduced from Fig. 8.

Figure 9 shows the SEM micrographs and EDS analysis results of the MT treated with 30 wt% addition of Na_2SiO_3 cured at 60 °C for 28 days. The higher magnification micrograph (see dash lines) shows that the particles are reacted on their surface and bonded to each other, showing coherent correlation in the structure. Furthermore, the dense structure formed in AAMT with 30 wt% Na_2SiO_3 at 60 °C (Fig. 9a and b) and it looks slightly different from the same sample which cured at 40 °C (Fig. 7d). It is worth noting that the structure is consistent with the compressive strength changes of AAMTs prepared at different conditions. The EDS analysis results indicate the presence of Na, Si, Ca, Mg, Fe, and a tiny amount of Al, which is confirmed by EDS elemental mapping of identified elements (Figs. 9 (c, d)). The Pyrrhotite and Magnetite can be identified in the raw materials (MT) and the presence of the small isolated spots of Fe ions in Fig. 8c could be a possible role of Fe in the EDX imaging.

Water Absorption

The effect of the alkali-activated additive on absorbability of the specimens cured for 28 days at 40 °C and 60 °C are shown in Fig. 10. This calculation provides an indirect approach to estimating the porosity network and idea about the influences of using different alkaline activator contents and curing regimes on the pore structure of the compositions. As was predicted (and as revealed in the results in Fig. 10), curing conditions affected pore structure, so that the water absorption varied in the range of 10–17%. Moreover, the water absorption of the specimens decreased with the higher Na_2SiO_3 concentration, which indicates a denser structure (less porosity) [45, 58]. Interestingly, it was observed that increasing the content of sodium silicate solution reduced the water absorption which could explain the slight increase in compressive strength. The minimum water absorption of the 28-day cured specimen at 40 °C and 60 °C came from AAMT with 30 wt% Na_2SiO_3 (12.62% and 9.98%, respectively), indicating a higher degree of reaction compared with other specimens and resulting in the highest compressive strength (15.84 and 22 MPa). When the MT is activated with a high amount of Na_2SiO_3 solution, the resulting material develops a very dense structure with the lowest apparent porosity. In fact, good correlation is observed mostly between compressive strength and water absorption in AAMT. Consequently, increasing the Na_2SiO_3 contents and curing temperature have led to escalate the amount of soluble silica in the mixture and finally accelerating the alkali activation process.

According to the successful usage of alkali activation technology in low-alumina mine tailings to produce sustainable construction materials, it is also proposed to use these materials in the production of lightweight thermal and acoustic panels. These materials use the combined advantages of alkali-activated binders, lightweight, good thermal resistance, and high sound absorption [59–68].

Conclusions

The promising experimental results from this study indicate that MT can be used to produce AAMTs as a potential sustainable material for operation or closure of mines. Stabilization of mine tailings using Na_2SiO_3 activation solution transforms such waste into a composition with adequate strength. This article reported the special effects of alkali activator concentration and curing time and temperature on the mechanical properties, microstructure, elemental and phase composition of AAMTs. The

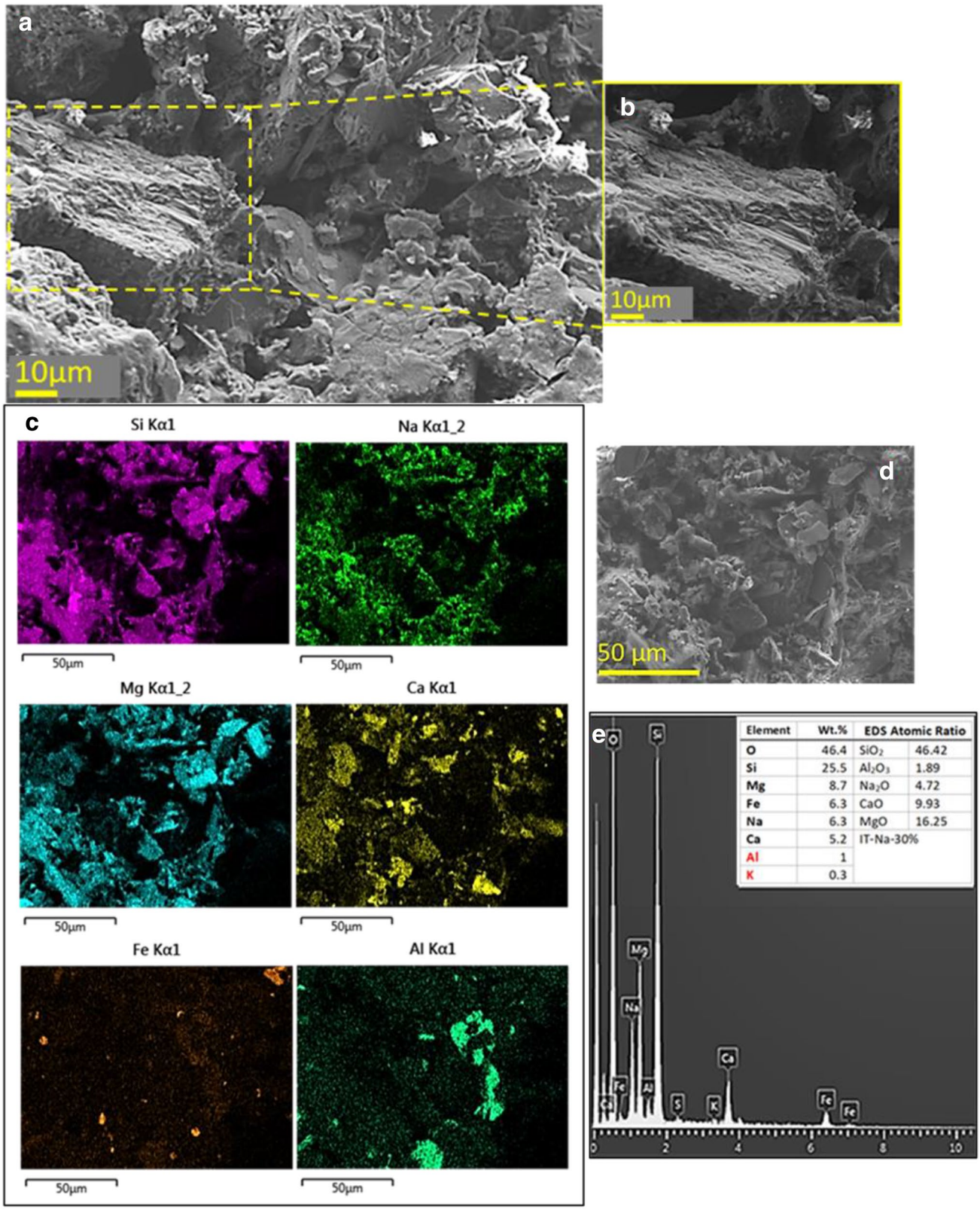

Fig. 9 **a, b** SEM micrograph of MT-30% Na_2SiO_3 cured at 60 °C for 28 days, the image 8b shows the highlighted area in the 8a at a higher magnification, **d** backscattered electron image a and **c**, **e** EDS element map and EDS spectra analysis of the backscattered electron image (Fig. 8d)

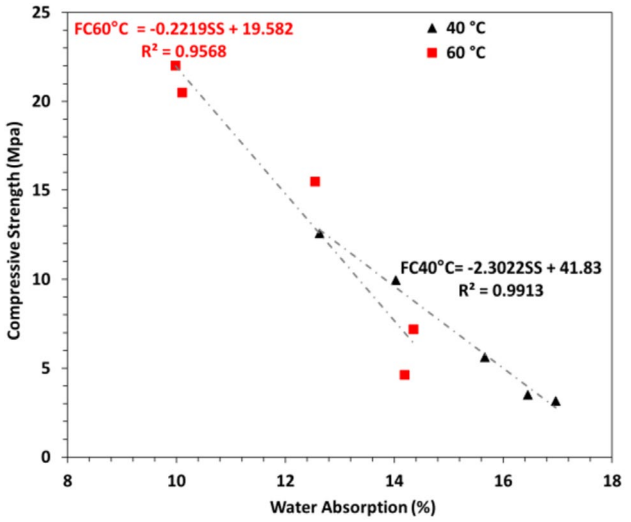

Fig. 10 The effect of the curing conditions at 40 °C and 60 °C on water absorption and compressive strength of AAMT

feasibility of developed AAMTs was studied by conducting compressive tests, water absorption tests, SEM imaging, and XRD analysis.

Na_2SiO_3 concentration and curing temperature/time are the factors that affect the compressive strength and microstructural properties of AAMTs. The SEM/EDS results indicate a heterogeneous matrix for AAMTs. The matrix is denser at higher curing temperatures. The XRD patterns at the optimum conditions show a change in both amorphous and crystalline phases, and the compressive strength is improved at elevated curing temperatures.

The ideal curing temperature (i.e., the curing temperature at the maximum compressive strength) depends on the Na_2SiO_3 concentration. The compressive strength increased with the increase of alkaline solution addition from 10 to 30 wt%. More Na_2SiO_3 addition and a higher curing temperature contribute to the dissolution of silica and subsequent formation of a higher amount of alkali-activated gels, resulting in a higher compressive strength. Among the mixtures examined in this study, the mixtures having 30 wt% Na_2SiO_3 solution can be considered the optimum mixture for reasonable compressive strength under the curing conditions studied here. The highest compressive strength of AAMT samples after 28 days of curing at 40 °C and 60 °C reached 14.78 and 20.49 MPa, respectively. The addition of Na_2SiO_3 to the MT results in higher compressive strength and lower water absorption.

Acknowledgements Open access funding provided by University of Oulu including Oulu University Hospital. The authors honestly appreciate European Union's Horizon 2020 Research and Innovation program to support this study under Grant Agreement ID: 730480, ITERAMS project.

References

1. Ahmari, S., Parameswaran, K., Zhang, L.: Alkali activation of copper mine tailings and low-calcium flash-furnace copper smelter slag. J. Mater. Civ. Eng. **27**, 04014193 (2015). https://doi.org/10.1061/(ASCE)MT.1943-5533.0001159
2. R.J. Collins, S.K. Ciesielski, L.S. Mason, Recycling and use of waste materials and by-products in highway construction: A synthesis of highway practice. Final report, (1993). https://www.osti.gov/biblio/7021109 (accessed November 2, 2018).
3. Zhang, L., Ahmari, S., Zhang, J.: Synthesis and characterization of fly ash modified mine tailings-based geopolymers. Constr. Build. Mater. **25**, 3773–3781 (2011). https://doi.org/10.1016/J.CONBUILDMAT.2011.04.005
4. Ahmari, S., Zhang, L.: Utilization of cement kiln dust (CKD) to enhance mine tailings-based geopolymer bricks. Constr. Build. Mater. **40**, 1002–1011 (2013). https://doi.org/10.1016/J.CONBUILDMAT.2012.11.069
5. IAEA (2004) The long term stabilization of uranium mill tailings. Doi:10.1016/j.jenvrad.2004.01.030.
6. Lange, L.C., Hills, C.D., Poole, A.B.: Preliminary investigation into the effects of carbonation on cement-solidified hazardous wastes. Environ. Sci. Technol. **30**, 25–30 (1996). https://doi.org/10.1021/es940702m
7. Ahmari, S., Zhang, L.: Durability and leaching behavior of mine tailings-based geopolymer bricks. Constr. Build. Mater. **44**, 743–750 (2013). https://doi.org/10.1016/J.CONBUILDMAT.2013.03.075
8. Majidi, B.: Geopolymer technology, from fundamentals to advanced applications: a review. Mater. Technol. **24**, 79–87 (2009). https://doi.org/10.1179/175355509X449355
9. Drechsler M, Graham A (2005) Geopolymers—an innovative materials technology bringing resource sustainability to construction and mining industries. 48th Institute of Quarrying Conference. Doi:10.13140/2.1.4108.8006.
10. van Deventer, J.S.J., Provis, J.L., Duxson, P., Lukey, G.C.: Reaction mechanisms in the geopolymeric conversion of inorganic waste to useful products. J. Hazard. Mater. **139**, 506–513 (2007). https://doi.org/10.1016/J.JHAZMAT.2006.02.044
11. Görhan, G., Kürklü, G.: The influence of the NaOH solution on the properties of the fly ash-based geopolymer mortar cured at different temperatures. Compos. Part B Eng. **58**, 371–377 (2014). https://doi.org/10.1016/J.COMPOSITESB.2013.10.082
12. Leong, H.Y., Ong, D.E.L., Sanjayan, J.G., Nazari, A.: The effect of different Na2O and K2O ratios of alkali activator on compressive strength of fly ash based-geopolymer. Constr. Build. Mater. **106**, 500–511 (2016). https://doi.org/10.1016/J.CONBUILDMAT.2015.12.141
13. Hajimohammadi, A., van Deventer, J.S.J.: Dissolution behaviour of source materials for synthesis of geopolymer binders: a kinetic approach. Int. J. Miner. Process. **153**, 80–86 (2016). https://doi.org/10.1016/J.MINPRO.2016.05.014
14. Duxson, P., Provis, J.L., Lukey, G.C., Mallicoat, S.W., Kriven, W.M., van Deventer, J.S.J.: Understanding the relationship

between geopolymer composition, microstructure and mechanical properties. Colloids Surf. A **269**(1–3), 47–58 (2005)
15. Fernández-Jiménez, A., Palomo, A.: Characterisation of fly ashes potential reactivity as alkaline cements☆. Fuel **82**(18), 2259–2265 (2003)
16. Hajimohammadi, A., van Deventer, J.S.J.: Solid reactant-based geopolymers from rice hull ash and sodium aluminate. Waste Biomass Valoriz. **8**(6), 2131–2140 (2017)
17. Palomo, A., Grutzeck, M.W., Blanco, M.T.: Alkali-activated fly ashes: a cement for the future. Cem. Concr. Res. **29**(8), 1323–1329 (1999)
18. Lloyd, R.R., Provis, J.L., van Deventer, J.S.J.: Microscopy and microanalysis of inorganic polymer cements 2: the gel binder. J. Mater. Sci. **44**(2), 620–631 (2009)
19. Hajimohammadi, A., Provis, J.L., van Deventer, J.S.J.: One-part geopolymer mixes from geothermal silica and sodium aluminate, industrial & engineering chemistry research. Am Chem Soc **47**(23), 9396–9405 (2008). https://doi.org/10.1021/ie8006825
20. Abdollahnejad, Z., et al.: Fiber-reinforced one-part alkali-activated slag/ceramic binders. Ceramics International. Elsevier **44**(8), 8963–8976 (2018). https://doi.org/10.1016/J.CERAMINT.2018.02.097
21. Abdollahnejad, Z., et al.: Development of one-part alkali-activated ceramic/slag binders containing recycled ceramic aggregates. J Mater Civ Eng **31**(2), 04018386 (2019). https://doi.org/10.1061/(ASCE)MT.1943-5533.0002608
22. Luukkonen, T., et al.: Comparison of alkali and silica sources in one-part alkali-activated blast furnace slag mortar. J. Clean. Prod. **187**, 171–179 (2018). https://doi.org/10.1016/J.JCLEPRO.2018.03.202
23. Luukkonen, T., et al.: One-part alkali-activated materials: a review. Cem. Concr. Res. **103**, 21–34 (2018). https://doi.org/10.1016/J.CEMCONRES.2017.10.001
24. Najafi Kani, E., Allahverdi, A., Provis, J.L.: Efflorescence control in geopolymer binders based on natural pozzolan. Cement and Concrete Composites. Elsevier **34**(1), 25–33 (2012). https://doi.org/10.1016/J.CEMCONCOMP.2011.07.007
25. Zhang, Z., et al.: Fly ash-based geopolymers: the relationship between composition, pore structure and efflorescence. Cem. Concr. Res. **64**, 30–41 (2014). https://doi.org/10.1016/J.CEMCONRES.2014.06.004
26. Ranjbar, N., et al.: A comprehensive study of the polypropylene fiber reinforced fly ash based geopolymer. PLoS ONE **11**(1), e0147546 (2016)
27. Yao, X., Yang, T., Zhang, Z.: Compressive strength development and shrinkage of alkali-activated fly ash–slag blends associated with efflorescence. Mater. Struct. **49**(7), 2907–2918 (2016). https://doi.org/10.1617/s11527-015-0694-3
28. Abdollahnejad, Z., Mastali, M., et al.: Comparative study on the effects of recycled glass-fiber on drying shrinkage rate and mechanical properties of the self-compacting mortar and fly ash-slag geopolymer mortar. J Mater Civ Eng **29**(8), 04017076 (2017). https://doi.org/10.1061/(ASCE)MT.1943-5533.0001918
29. Kheradmand, M., et al.: Experimental and numerical investigations on the flexural performance of geopolymers reinforced with short hybrid polymeric fibres. Compos. Part B **126**, 108–118 (2017). https://doi.org/10.1016/J.COMPOSITESB.2017.06.001
30. Kheradmand, M., Abdollahnejad, Z., Pacheco-Torgal, F.: Shrinkage performance of fly ash alkali-activated cement based binder mortars. KSCE **22**(5), 1854–1864 (2018). https://doi.org/10.1007/s12205-017-1714-3
31. Mastali, M., Kinnunen, P., Dalvand, A., et al.: Drying shrinkage in alkali-activated binders—a critical review Constr. Build. Mater. **190**, 533–550 (2018). https://doi.org/10.1016/J.CONBUILDMAT.2018.09.125
32. Abdollahnejad, Z., Pacheco-Torgal, F., de Aguiar, J.B.: Development of foam one-part geopolymers with enhanced thermal insulation performance and low carbon dioxide emissions. Adv. Mater. Res.**1129**, 565–572 (2015). https://doi.org/10.4028/www.scientific.net/AMR.1129.565
33. Zachiarias Z, Agioutantis K, Komnitsas K (2006) Proceedings of the 2nd international conference on advances in mineral resources management and environmental geotechnology (AMIREG 2006): 25–27 September 2006, Hania, Greece, Heliotopos Conferences, 2006.
34. Kinnunen, P., Ismailov, A., Solismaa, S., Sreenivasan, H., Räisänen, M.-L., Levänen, E., Illikainen, M.: Recycling mine tailings in chemically bonded ceramics—a review. J. Clean. Prod. **174**, 634–649 (2018). https://doi.org/10.1016/j.jclepro.2017.10.280
35. Feng Q (2015) Applying mine tailing and fly ash as construction materials for a sustainable development. https://repository.arizona.edu/handle/10150/594926 (accessed November 2, 2018)
36. Ahmari, S., Zhang, L., Zhang, J.: Effects of activator type/concentration and curing temperature on alkali-activated binder based on copper mine tailings. J. Mater. Sci. **47**, 5933–5945 (2012). https://doi.org/10.1007/s10853-012-6497-9
37. Barnhisel, R.I., Darmody, R.G., Daniels, W.L., Skousen, J.G., Sexstone, A., Ziemkiewicz, P.F.: Acid mine drainage control and treatment. Reclam, pp. 131–168. American Society of Agronomy, Crop Science Society of America, Soil Science Society of America, Drastically Disturb. Lands (1996)
38. Pacheco-Torgal, F., Castro-Gomes, J., Jalali, S.: Properties of tungsten mine waste geopolymeric binder. Constr. Build. Mater. **22**, 1201–1211 (2008). https://doi.org/10.1016/J.CONBUILDMAT.2007.01.022
39. Fernando, P.-T., João, C.-G., Said, J.: Durability and environmental performance of alkali-activated tungsten mine waste mud mortars. J. Mater. Civ. Eng. **22**, 897–904 (2010). https://doi.org/10.1061/(ASCE)MT.1943-5533.0000092
40. Yu, L., Zhang, Z., Huang, X., Jiao, B., Li, D., Yu, L., Zhang, Z., Huang, X., Jiao, B., Li, D.: Enhancement experiment on cementitious activity of copper-mine tailings in a geopolymer system. Fibers. **5**, 47 (2017). https://doi.org/10.3390/fib5040047
41. Khale, D., Chaudhary, R.: Mechanism of geopolymerization and factors influencing its development: a review. J. Mater. Sci. **42**, 729–746 (2007). https://doi.org/10.1007/s10853-006-0401-4
42. Pacheco-Torgal, F., Castro-Gomes, J.P., Jalali, S.: Investigations on mix design of tungsten mine waste geopolymeric binder. Constr. Build. Mater. **22**, 1939–1949 (2008). https://doi.org/10.1016/J.CONBUILDMAT.2007.07.015
43. ASTM C293/C293M-16 (2016) Standard test method for flexural strength of concrete (using simple beam with center-point loading), International, A.S.T.M., West Conshohocken, PA. https://www.astm.org
44. ASTM C116–90 (1999) Test method for compressive strength of concrete using portions of beams broken in flexure (Withdrawn 1999), (n.d.). https://www.astm.org/Standards/C116.htm (accessed November 8, 2018)
45. Plastics—determination of water absorption. BS EN ISO (1999) 62:1–8.
46. Ghafoori, N., Najimi, M., Radke, B.: Natural pozzolan-based geopolymers for sustainable construction. Environ. Earth Sci. **75**(14), 1110 (2016)
47. Fernández-Jiménez, A., Palomo, A., Criado, M.: Microstructure development of alkali-activated fly ash cement: a descriptive model. Cem. Concr. Res. **35**, 1204–1209 (2005). https://doi.org/10.1016/j.cemconres.2004.08.021
48. Lothenbach, B., Nied, D., L'Hôpital, E., Achiedo, G., Dauzères, A.: Magnesium and calcium silicate hydrates. Cem. Concr. Res. **77**, 60–68 (2015)

49. Pytel Z, Malolepszy J (1997). In: Justnes H (ed) Proc Int Congr Chem Cem 10th, Amarkai AB, Goeteborg.
50. Kovalchuk, G., Fernández-Jiménez, A., Palomo, A.: Alkali-activated fly ash: effect of thermal curing conditions on mechanical and microstructural development—part II. Fuel **86**(3), 315–322 (2007)
51. Duxson, P., Provis, J.L., Lukey, G.C., van Deventer, J.S.J.: The role of inorganic polymer technology in the development of "green concrete". Cem. Concr. Res. **37**, 1590–1597 (2007). https://doi.org/10.1016/j.cemconres.2007.08.018
52. Zeng, X., Wu, J., Rohlf, R.: Modeling the seismic response of coal-waste tailings dams. Geotech. News **6**(6), 29–32 (1998)
53. Shen L, Farid H, Mcpeek MA (2008) [No Title], In: Evolution (N. Y). MATEC Web of Conference, Covilhã, p 1–14.
54. Bernal, S.A., Provis, J.L., Walkley, B., San Nicolas, R., Gehman, J.D., Brice, D.G., Kilcullen, A.R., Duxson, P., van Deventer, J.S.J.: Gel nanostructure in alkali-activated binders based on slag and fly ash, and effects of accelerated carbonation. Cem. Concr. Res. **53**, 127–144 (2013)
55. Karim, M.E., Alam, M.J.: Effect of non-plastic silt content on the liquefaction behavior of sand-silt mixture. Soil Dyn. Earthq. Eng. **65**, 142–150 (2014). https://doi.org/10.1016/j.soildyn.2014.06.010
56. Temuujin, J., van Riessen, A., Williams, R.: Influence of calcium compounds on the mechanical properties of fly ash geopolymer pastes. J. Hazard. Mater. **167**, 82–88 (2009). https://doi.org/10.1016/j.jhazmat.2008.12.121
57. Kastiukas, G., Zhou, X.: Effects of waste glass on alkali-activated tungsten mining waste: composition and mechanical properties. Mater. Struct. **50**, 194 (2017). https://doi.org/10.1617/s11527-017-1062-2
58. Méndez-Ortiz, B.A., Carrillo-Chávez, A., Monroy-Fernández, M.G.: Acid rock-drainage and metal leaching from mine waste material (tailings) of a Pb–Zn–Ag skarn deposit: environmental assessment through static and kinetic laboratory tests. Rev. Mex. Ciencias Geol. **24**(2), 161–169 (2007)
59. Zhang, Z., et al.: Geopolymer foam concrete: an emerging material for sustainable construction. Constr. Build. Mater. **56**, 113–127 (2014). https://doi.org/10.1016/J.CONBUILDMAT.2014.01.081
60. Zhang, Z., et al.: Mechanical, thermal insulation, thermal resistance and acoustic absorption properties of geopolymer foam concrete. Cem. Concr. Compos.**62**, 97–105 (2015). https://doi.org/10.1016/J.CEMCONCOMP.2015.03.013
61. Abdollahnejad, Z., et al.: Mix design, properties and cost analysis of fly ash-based geopolymer foam. Constr. Build. Mater. **80**, 18–30 (2015). https://doi.org/10.1016/J.CONBUILDMAT.2015.01.063
62. Abdollahnejad, Z., Miraldo, S., et al.: Cost-efficient one-part alkali-activated mortars with low global warming potential for floor heating systems applications. Eur. J. Environ. Civ. Eng. **21**(4), 412–429 (2017). https://doi.org/10.1080/19648189.2015.1125392
63. Hajimohammadi, A., Ngo, T., Mendis, P., Kashani, A., et al.: Alkali activated slag foams: the effect of the alkali reaction on foam characteristics. J. Clean. Prod. **147**, 330–339 (2017). https://doi.org/10.1016/J.JCLEPRO.2017.01.134
64. Hajimohammadi, A., Ngo, T., Mendis, P., Nguyen, T., et al.: Pore characteristics in one-part mix geopolymers foamed by H2O2: the impact of mix design. Mater. Design**130**, 381–391 (2017). https://doi.org/10.1016/J.MATDES.2017.05.084
65. Mastali, M., Kinnunen, P., Isomoisio, H., et al.: Mechanical and acoustic properties of fiber-reinforced alkali-activated slag foam concretes containing lightweight structural aggregates. Constr. Build. Mater. **187**, 371–381 (2018). https://doi.org/10.1016/J.CONBUILDMAT.2018.07.228
66. Mastali, M., et al.: Impacts of casting scales and harsh conditions on the thermal, acoustic, and mechanical properties of indoor acoustic panels made with fiber-reinforced alkali-activated slag foam concretes. Mater. Multidiscip. Dig. Pub. Inst.**12**(5), 825 (2019). https://doi.org/10.3390/ma12050825
67. Abdollahnejad, Z., Luukkonen, T., Mastali, M., Giosue, C., Favoni, O., Ruello, M.L., Kinnunen, P., Illikainen, M.: Microstructural analysis and strength development of one-part alkali-activated slag/ceramic binders under different curing regimes. Waste Biomass Valoriz. (2019). https://doi.org/10.1007/s12649-019-00626-9
68. Nazari, A., Sanjayan, J.G., Zhang, Z., Yang, T., Wang, H.: Alkali-activated cement (AAC) from fly ash and high-magnesium nickel slag. Handb. Low Carbon Concr. (2017). https://doi.org/10.1016/B978-0-12-804524-4.00013-0

Affiliations

Mahroo Falah[1] · Robert Obenaus-Emler[2] · Paivo Kinnunen[1] · Mirja Illikainen[1]

✉ Mahroo Falah
mahroo.falahpoorsichani@oulu.fi

Robert Obenaus-Emler
robert.emler@unileoben.ac.at

Paivo Kinnunen
Paivo.Kinnunen@oulu.fi

Mirja Illikainen
Mirja.Illikainen@oulu.fi

[1] Fibre and Particle Engineering, Faculty of Technology, University of Oulu, 90014 Oulu, Finland

[2] Chair of Ceramics, Montanuniversitaet Leoben, 8700 Leoben, Austria